25th IMEKO TC4 International Symposium
23rd International Workshop on ADC and DAC Modelling and Testing
IMEKO TC-4 2022
Brescia, Italy / September 12-14, 2022

Numerical Modelling of the Magnetic Fields Generated by Underground Power Cables with Two-point Bonded Shields

Eduard Lunca[1], Silviu Vornicu[2], Alexandru Salceanu[3]

[1]Faculty of Electrical Engineering, 23 Prof. Dimitrie Mangeron Blvd., 700050 Iasi, Romania, elunca@tuiasi.ro, +40 232701246
[2]Faculty of Electrical Engineering, 23 Prof. Dimitrie Mangeron Blvd., 700050 Iasi, Romania, silviusieca@gmail.com, +40 232701246
[3]Faculty of Electrical Engineering, 23 Prof. Dimitrie Mangeron Blvd., 700050 Iasi, Romania, asalcean@tuiasi.ro, +40 232701157

***Abstract* – In this study we present a 2D finite element model for computing magnetic fields generated by underground power cables with two-point bonded shields. The model is developed in ANSYS Maxwell 2D low-frequency electromagnetic field simulation software for a typical 12/20 kV three-phase underground power cable system in flat formation, but it can be adapted to any line. The model validation is achieved by analytical computations conducted with a software tool based on the Biot-Savart law and superposition principle. RMS magnetic flux density profiles calculated at various heights above the ground with these two methods correlate very well. This is also true for induced shield currents.**

I. INTRODUCTION

The continuous development of urban centers leads to an increase in the demand for electricity, hence underground power cables (UPCs) are becoming more frequent in these places. It is well known that, similar to overhead power lines, UPCs generate low-frequency electric and magnetic fields. The electric fields are nearly completely eliminated by the surrounding metallic sheath(s) and the conducting soil. In contrast, the magnetic fields are not shielded and reduce only by distance. In fact, the magnetic fields from an UPC sometimes can be stronger than those generated by a corresponding overhead power line because these lines are located farther away from ground [1,2].

Calculating magnetic fields from UPCs is very important in several research areas, including human exposure evaluation studies [3-8]. A common 2D approach is based on the Biot-Savart law and superposition principle, assuming that the conductors are straight, horizontal, infinitely long and parallel to each other and the effect of the induced shield currents on the magnetic field is negligible. However, when dealing with solid bonding (i.e., the underground cables operate with their metallic shields bonded and grounded at both ends), the circulating currents induced in shields may achieve the same order as the wire-core currents, which leads to a weakening of the total magnetic field. In some references, e.g. [9] and [10], analytical expressions for the induced shield currents have been obtained under balanced three-phase conditions. It has also been considered the magnetic field reduction.

Some finite element models have also been developed for computing magnetic fields from UPCs with two-point bonded shields. An extensive study is presented in [11], which uses COMSOL Multiphysics to investigate the magnetic field reduction rate for a three-phase flat cable system as a function of the distance between cables, the shield diameter, as well as the cross-sectional area of the cable shields. In [12], QuickField was mainly used for predicting underground cable ampacity (for both flat and trefoil formations), while the developed 2D model also allows investigating the magnetic field distribution at the ground surface. Another study to be mentioned is [13], in which ANSYS Maxwell 2D was used for studying loss reduction in cable sheathing and, in much lesser extent, magnetic field distribution close to the ground surface.

In our study, the problem of the magnetic field from underground power cables with two-point bonded shields is also solved using ANSYS Maxwell 2D. The proposed model is developed for a typical 12/20 kV three-phase underground power cable system in flat formation, but it can be adapted to any line. For validation, calculated magnetic fields are checked against analytical results obtained with a software tool based on the Biot-Savart law and superposition principle, which represents an updated version of a previously developed program [2].

The rest of the paper is structured as follows: Section II presents the geometry and simulation conditions for the

UPC system considered for analysis; Section III describes the proposed finite element model; Section IV deals with model validation; Section V discusses numerical simulation results; Section V draws conclusions.

II. UNDERGROUND POWER CABLE SYSTEM SELECTED FOR ANALYSIS

The basic geometry of the three-phase cable system selected for analysis is presented in Fig. 1a. It consists of three NA2XS(FL)2Y 12/20 kV single-core medium voltage cables in flat formation, separated by a distance between centers of 0.1 m and buried in the ground at a depth of 0.8 m. Each cable has an aluminum (Al) core conductor with the cross-sectional area of 150 mm^2 and a copper (Cu) wire shield with the cross-sectional area of 25 mm^2. The copper shields are grounded at the ends of the cables as depicted in Fig. 1b. For computation, it is assumed that the three-phase UPC system has balanced currents, as follows: $\underline{I}_1$ = 100 A ∠ -120°, $\underline{I}_2$ = 100 A ∠ 0° and $\underline{I}_3$ = 100 A ∠ 120°. The simulation temperature is set to 22 °C, which is default in ANSYS Maxwell 2D.

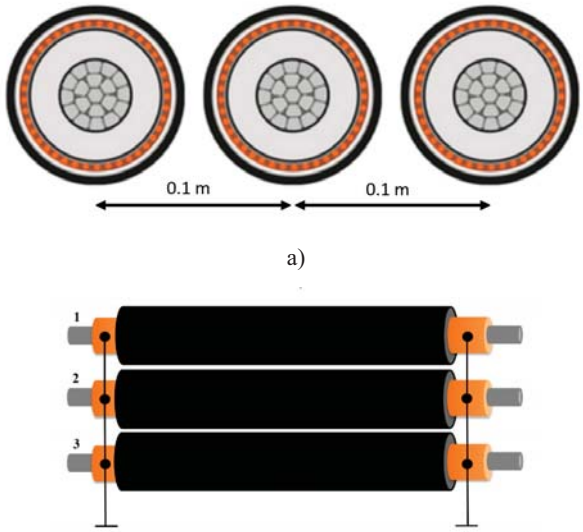

Fig. 1. Three-phase UPC system: a) basic geometry; b) two-point bonding scheme

III. FINITE ELEMENT MODEL

ANSYS Maxwell 2D is a software package that uses finite element method (FEM) to solve 2D low-frequency electromagnetic problems, by specifying the appropriate geometry, material properties and excitations for a device or system of devices – in our case, a three-phase underground power cable system. The proposed problem is solved using the "eddy current solver", which allows computing steady state, time-varying (AC) magnetic fields at a given frequency, here 50 Hz.

The global FEM model is illustrated in Fig. 2a, where the computational domain is a square of side a = 40 m, sufficiently large to determine the behavior of the magnetic field well outside from the centerline. The three-phase UPC system is buried – at the mentioned depth – in a ground with the electrical conductivity σ = 0.05 S/m and the relative magnetic permeability μ_r = 1. Each power cable is modeled as presented in Fig. 2.b, using a simplified 4-layer cable model consisting of Al core conductor ($\sigma = 34.45 \cdot 10^6$ S/m and $\mu_r = 1$), XLPE insulation ($\sigma = 1 \cdot 10^{-15}$ S/m and $\mu_r = 1$), Cu shield ($\sigma = 58 \cdot 10^6$ S/m and $\mu_r = 1$) and HDPE cover ($\sigma = 1 \cdot 10^{-14}$ S/m and $\mu_r = 1$). The thickness (th) of the Cu shield layer is chosen so that it matches the specified 25 mm^2 cross-sectional area.

The values of the wire-core currents (amplitude and phase) are assigned using the software functionality "Current Excitation", whereas the shield bonding is encoded in the model by the coupled electrical circuit in Fig. 2c, where external windings are used for controlling the induced shield currents. This electrical circuit was defined with Maxwell Circuit Editor.

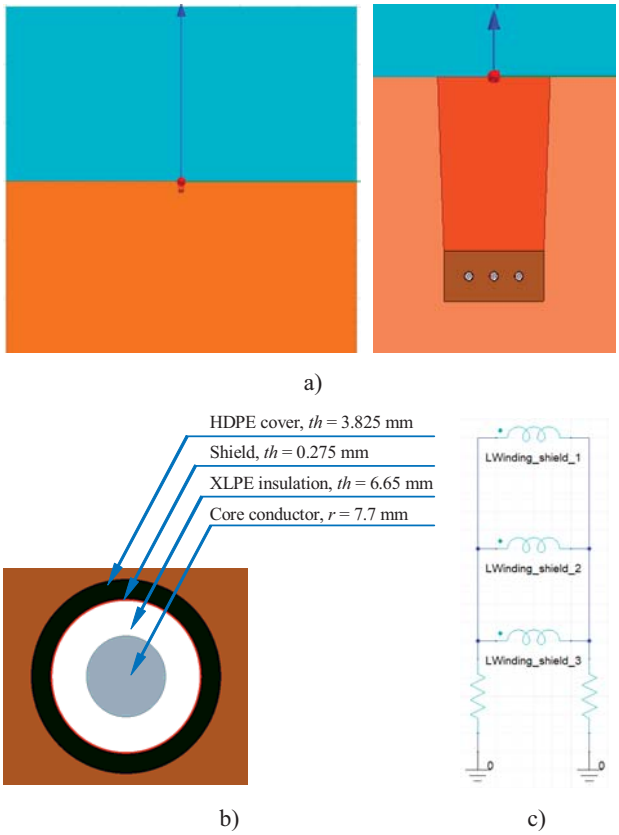

Fig. 2. ANSYS Maxwell 2D model for computing magnetic fields from power cables with two-point bonded shields: a) global geometric model; b) simplified cable model; c) coupled circuit for shield bonding

The applied boundary conditions are of Balloon type, which models the region outside the defined space as extending to infinity. In this case, the magnetic vector

potential, $\vec{A}$, goes to zero at infinity; the magnetic flux lines are neither tangential nor normal to the Balloon boundary [14].

A fine mesh was defined for analysis, totalizing a number of triangle elements in the order of 710000. The adaptive setup was configured with a maximum number of passes of 10 and a percent error of 0.1. The convergence was set as 30% refinement per pass, minimum number of passes of 2 and minimum converged passes of 1. The adaptive frequency was 50 Hz.

With this approach, ANSYS Maxwell 2D allowed us generating instantaneous magnetic flux density distributions in the cross section of the cable system (over a period of 20 ms), as presented in Fig. 3a. The RMS magnetic flux density at any desired height h above the ground is determined by importing a sufficiently large number of instantaneous magnetic flux density profiles (Fig. 3b) in Microsoft Excel, where they are summed together with the formula [15, 16]:

$$B_{RMS}(i) = \sqrt{\frac{1}{N}\sum_{n=1}^{N} B_n^2(i)}, \quad (1)$$

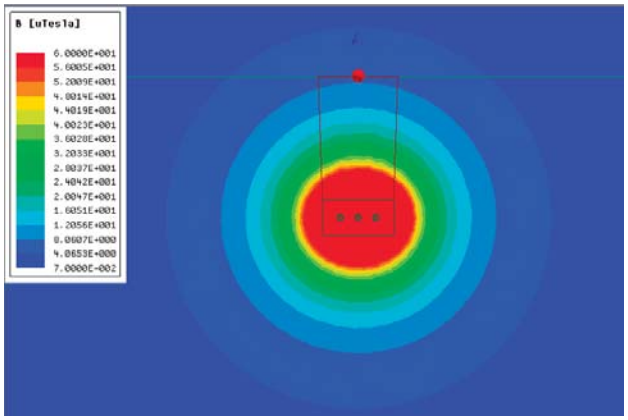

a)

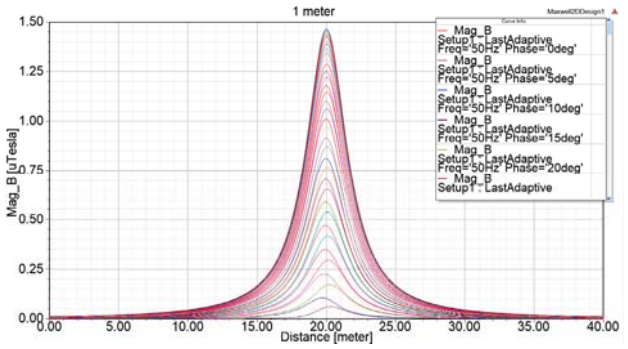

b)

Fig. 3. Example of simulation results: a) momentary magnetic field distribution in the cross section of the cable system (t = 15.55 ms); b) instantaneous magnetic flux density profiles at h = 1 m above the ground

where $B_1(i)$, …, $B_N(i)$ are the instantaneous values of the magnetic flux density corresponding to the point i of the profile and $N = 73$ is the total number of values. These results will be discussed in Section V.

IV. MODEL VALIDATION

In order to verify the numerical results obtained with the proposed FEM model, an interactive software tool based on the Biot-Savart law and superposition principle has been developed. Based on the assumptions in Section I, the total magnetic flux density at any measuring point (x, y) in the vicinity of the cable system can be calculated as:

$$\underline{B}_x = \sum_{i=1}^{3} \frac{-\mu_0}{2\pi}\left(\underline{I}_i + \underline{I}_{shi}\right)\left[\frac{y-y_i}{r_i^2}\right]; \quad (2)$$

$$\underline{B}_y = \sum_{i=1}^{3} \frac{\mu_0}{2\pi}\left(\underline{I}_i + \underline{I}_{shi}\right)\left[\frac{x-x_i}{r_i^2}\right]; \quad (3)$$

$$B = \sqrt{\left|\underline{B}_x\right|^2 + \left|\underline{B}_y\right|^2}, \quad (4)$$

where $\underline{I}_i$ is the phase current carried by the conductor located at (x_i, y_i), $\underline{I}_{shi}$ is the circulating current in the shield located at (x_i, y_i), $r_i = \sqrt{(x-x_i)^2 + (y-y_i)^2}$ represents the distance between the conductor/shield and the measurement point (x, y) and $\mu_0 = 4\pi \cdot 10^{-7}$ H/m is the magnetic permeability of the free space.

If assuming the same phase sequence ($\underline{I}_1 = I \angle -120°$, $\underline{I}_2 = I \angle 0°$ and $\underline{I}_3 = I \angle 120°$), it can be shown that the currents induced in the shields of a three-phase underground cable system in flat formation have the following expressions [17]:

$$\underline{I}_{sh1} = \frac{\underline{I}_2}{2}\left[\frac{Q^2}{R_{sh}^2+Q^2} - \frac{\sqrt{3}R_{sh}P}{R_{sh}^2+P^2} + j\left(\frac{R_{sh}Q}{R_{sh}^2+Q^2} + \frac{\sqrt{3}P^2}{R_{sh}^2+P^2}\right)\right]; \quad (5)$$

$$\underline{I}_{sh2} = -\underline{I}_2\left(\frac{Q^2}{R_{sh}^2+Q^2} + j\frac{R_{sh}Q}{R_{sh}^2+Q^2}\right); \quad (6)$$

$$\underline{I}_{sh3} = \frac{\underline{I}_2}{2}\left[\frac{Q^2}{R_{sh}^2+Q^2} + \frac{\sqrt{3}R_{sh}P}{R_{sh}^2+P^2} + j\left(\frac{R_{sh}Q}{R_{sh}^2+Q^2} - \frac{\sqrt{3}P^2}{R_{sh}^2+P^2}\right)\right], \quad (7)$$

where:

- R_{sh} is the shield resistance at the considered temperature, in Ω/m;
- $Q = X - \frac{X_m}{3} = \omega\left(M - \frac{M_m}{3}\right)$;
- $P = X + X_m = \omega(M + M_m)$;
- $M = 2 \cdot 10^{-7} \ln\left(\frac{s}{r_{sh}}\right)$, in H/m;
- $M_m = 2 \cdot 10^{-7} \ln 2$, in H/m.

In the expression of M above, s is the spacing between the centers of the adjacent conductors, in m, and r_{sh} is the mean of the outer and inner radii of the shield, also in m.

Finally, the shield resistance R_{sh} (at a shield temperature t_{sh}) is calculated with the formula:

$$R_{sh} = \frac{\rho_{sh20}}{A_{sh}}[1 + \alpha_{sh20}(t_{sh} - 20)], \qquad (8)$$

where ρ_{sh20} is the electrical resistivity of the shield material at 20 °C, A_{sh} is the shield cross-sectional area and α_{sh20} is the temperature coefficient of resistance at 20 °C. In our case, at t_{sh} = 22 °C, R_{sh} = 0.695 mΩ/m.

All these mathematical equations, together with a field mapping algorithm, have been implemented into a LabVIEW program that generates lateral profiles of the total RMS magnetic flux density, B, as well as of its transversal components, B_x and B_y, at any user-defined height above the ground. The program also displays the induced shield currents (RMS value and phase). Examples of magnetic flux density profiles generated with this simulation tool are presented in Fig. 4.

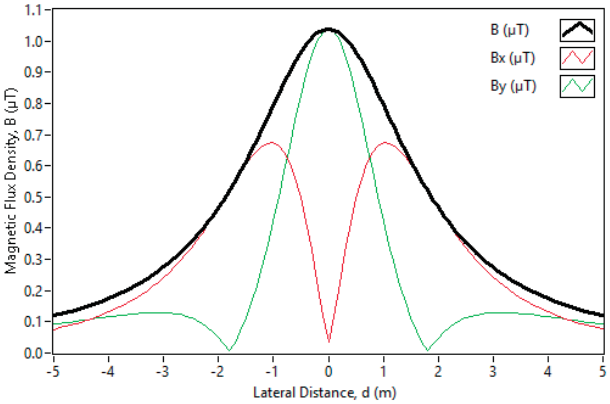

Fig. 4. The total RMS magnetic flux density and its transversal components at the height of 1 m above the ground (analytical computation)

V. RESULTS AND DISCUSSION

A comparison between numerical simulation results and analytical computation results (lateral profiles of the total RMS magnetic flux density at the height of 1 m above the ground, which is generally preferred in health-related exposure studies when dealing with power-frequency systems) is given in Fig. 5. Induced shield currents calculated by both methods are given in Table 1 and Table 2, respectively. As we can see, the results obtained by the two methods correlate very well.

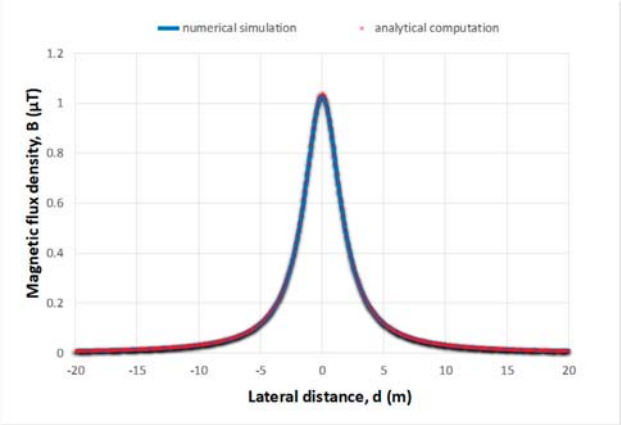

Fig. 5. Comparison between numerical and analytical results (RMS magnetic flux density profiles at the height of 1 m above the ground)

Table 1. Induced shield currents obtained by numerical simulation.

Current No.	$\underline{I}_{sh}$ (A)	RMS value (A)	Phase (°)
1	-18.40+j12.26	22.11	146.32
2	-2.35-j15.13	15.31	-98.83
3	20.75+j2.86	20.95	7.85

Table 2. Induced shield currents obtained by analytical computation.

Current No.	$\underline{I}_{sh}$ (A)	RMS value (A)	Phase (°)
1	-18.30+j12.13	21.96	146.46
2	-2.31-j15.02	15.21	-98.75
3	20.61+j2.89	20.82	7.99

Lateral profiles of the total RMS magnetic flux density at several heights above the ground, obtained by numerical simulation, are presented in Fig. 6. As it can be observed, the magnetic field at the centerline varies strongly, from 5.18 μT at 0 m to 0.63 μT at 1.5 m. Modifying the grounding resistance (see Fig. 2c) between 0.1 Ω and 50 Ω has virtually no effect on the magnetic field distribution.

Fig. 7 compares lateral profiles of the total RMS magnetic flux density computed with two-point bonded shields and non-bonded shields, respectively (h = 1 m). As shown in this figure, the underground cable system with two-point bonded shields produces a magnetic field that is 2.64% (2.63%, analytically) lower than the magnetic field created by the non-bonded cable system.

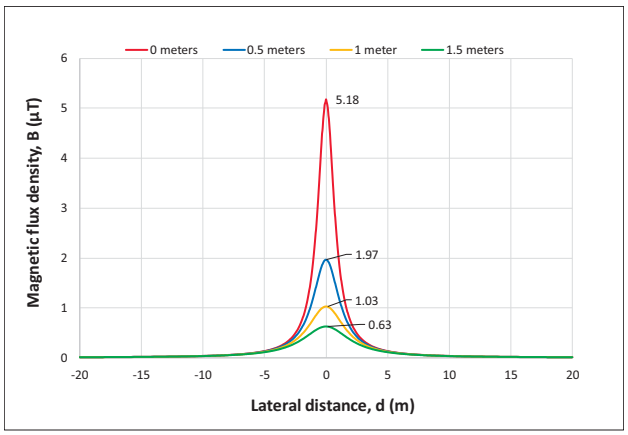

Fig. 6. Magnetic field from the three-phase underground cable system at several heights above the ground (numerical simulation)

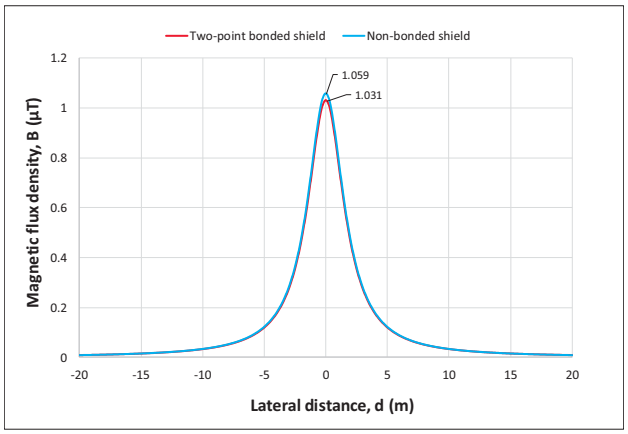

Fig. 7. Magnetic field from the three-phase phase underground cable system with two-point bonded shields and non-bonded shields, h = 1 m (numerical simulation)

Vertical profiles of the total RMS magnetic flux density at the centerline, obtained by numerical simulation, are presented in Fig. 8 (top dashed line – non-bonded cable system; bottom solid line – bonded cable system).

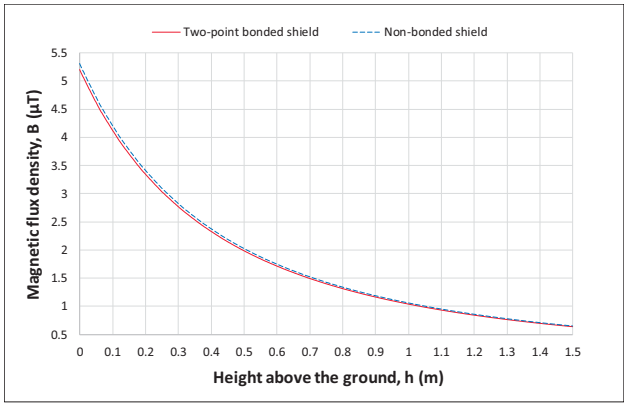

Fig. 8. Magnetic field at the centerline for two-point bonded shields and non-bonded shields (numerical simulation)

As it can be observed from the results presented above, the magnetic field reduction rate for the analyzed three-phase cable system is very low. However, for other cable systems, depending on their geometry and the cable characteristics, it may significantly increase.

VI. CONCLUSIONS

The main achievement of this study consists in the development and validation of a simple and effective ANSYS Maxwell 2D model for computing and analyzing magnetic fields generated by underground cable systems with two-point bonded shields. Comparisons to analytical computations based on the Biot-Savart law and superposition principle revealed a very good agreement between results. The proposed FEM model can be adapted to calculate magnetic field distributions for any three-phase cable layout, as well as for various cable groups, taking into account influencing factors such as cable spacing, burial depth, phase sequence, magnetic permeability of soil, etc.

REFERENCES

[1] EMFs.info, “Underground power cables”, online at https://www.emfs.info/sources/underground/ (Accessed April 2022).

[2] S. Vornicu, E. Lunca, A. Salceanu, “Computation of the Low Frequency Magnetic Fields Generated by a 12/20 kV Underground Power Line”, 2018 International Conference and Exposition on Electrical and Power Engineering (EPE), 2018, pp. 0630-0633.

[3] E. Fernandez, J. Patrick, “Magnetic Fields from High Voltage Power Cables”, online at https://elek.com.au/articles/magnetic-fields-from-high-voltage-power-cables/ (Accessed April 2022).

[4] V.J. Hernández Jiménez, E.D. Castronuovo, I. Sánchez Rodríguez-Morcillo, “Optimal statistical calculation of underground cable bundles positions for time-varying currents”, International Journal of Electrical Power & Energy Systems, Vol. 95, 2018, pp. 26-35.

[5] R. Djekidel, D. Mahi, S.A. Bessedik, C. Hadjaj, “Analysis of magnetic flux density generated by a three-phase underground power cable”, 10th National Conference on High Voltage (CNHT), 2016, pp. 1-6.

[6] K. Ates, H.F. Carlak, S. Ozen, “Magnetic Field Exposures due to Underground Power Cables: A Simulation Study”, 2nd World Congress on Electrical Engineering and Computer Systems and Science (EECSS’16), 2016, pp. 1-7.

[7] Z.A. Abu Zarim, T.M. Anthony, “Magnetic field simulation & measurement of underground cable system inside duct bank,” 22nd International Conference on Electricity Distribution, Stockholm, 2013, pp. 1-3.

[8] A.S. Farag, A.A. Hossam-Eldin, H.M. Karawia,

"Magnetic fields management for underground cables structures" 21st International Conference on Electricity Distribution Frankfurt (CIRED2011), 2011, pp 1-4.

[9] V. Rozov, V. Grinchenko, O. Tkachenko, A. Yerisov, "Analytical Calculation of Magnetic Field Shielding Factor for Cable Line with Two-Point Bonded Shields" IEEE 17th International Conference on Mathematical Methods in Electromagnetic Theory (MMET), 2018, pp. 358-361.

[10] J.R. Riba Ruiz, X. Alabern Morera, "Effects of the circulating sheath currents in the magnetic field generated by an underground power line", International Conference on Renewable Energy and Power Quality, 2006, pp. 1-5.

[11] V. Grinchenko, O. Tkachenko, K. Chunikhin, "Magnetic field calculation of cable line with two-point bonded shields", IEEE Int. Young Scientists Forum on Applied Physics and Engineering, 2017, pp. 211-214.

[12] S. Dubitsky, G. Greshnyakov, N. Korovkin, "Refinement of underground power cable ampacity by multiphysics FEA simulation", International Journal of Energy, Vol. 9, 2015, pp. 12-19.

[13] B. Novák, L. Koller, I. Berta, "Loss reduction in cable sheathing", International Conference on Renewable Energies and Power Quality (ICREPQ'10), 2010, pp. 293-297.

[14] S. Fericean, "Inductive Sensors for Industrial Applications", Artech House, Norwood, 2019.

[15] E. Lunca, B.C. Neagu, S. Vornicu, "Finite Element Analysis of Electromagnetic Fields Emitted by Overhead High-Voltage Power Lines", in *Numerical Methods for Energy Applications*, Springer, Cham, 2021.

[16] S. Vornicu, E. Lunca, A. Salceanu, "ANSYS Maxwell Finite Element Model for 2D Computation of the Magnetic Field Generated by Overhead High-Voltage Power Lines," 2019 International Conference on Electromechanical and Energy Systems (SIELMEN), 2019, pp. 1-4.

[17] O.E. Gouda, "Environmental Impacts on Underground Power Distribution", 1st edition, IGI Global, 2016.